Extending the Bandwidth of Reverse Saturable Absorption in Platinum Complexes Using Two-Photon-Initiated Excited-State Absorption

Bingguang Zhang,[†] Yunjing Li,[†] Rui Liu,[†] Timothy M. Pritchett,[‡] Joy E. Haley,[§] and Wenfang Sun*[,†]

[†]Department of Chemistry and Biochemistry, North Dakota State University, Fargo, North Dakota 58108-6050, United States
[‡]U.S. Army Research Laboratory, AMSRD-SEE-M, 2800 Powder Mill Road, Adelphi, Maryland 20783-1197, United States
[§]Materials and Manufacturing Directorate, Air Force Research Laboratory, Wright Patterson Air Force Base, Dayton, Ohio 45433, United States

Ⓢ *Supporting Information*

ABSTRACT: Pt(II) complexes bearing 4-(7-(benzothiazol-2′-yl)-9,9-diethyl-fluoren-2-yl)-2,2′:6′,2″-terpyridine or 4-(7-(benzothiazol-2′-yl)-9,9-diethylfluoren-2-yl)ethynyl-2,2′:6′,2″-terpyridine ligand exhibit strong reverse saturable absorption in the visible spectral region and large two-photon initiated excited-state absorption in the near-IR region. They are promising broadband nonlinear absorbing materials from the visible to the near-IR region. The extended π-conjugation in complex **2** that has a C≡C linker between the terpyridine ligand and the 4-(7-(benzothiazol-2′-yl)-9,9-diethylfluoren-2-yl) substituent significantly increases the two-photon absorption cross sections (σ_2), making it among the strongest of two-photon absorbing Pt(II) complexes.
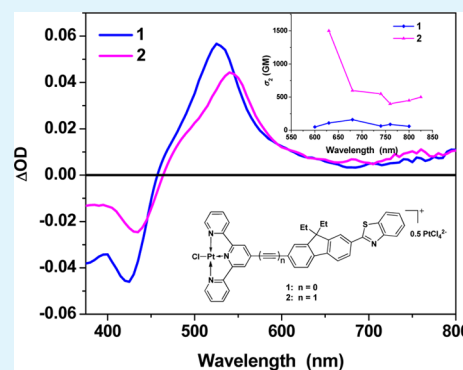
1. INTRODUCTION

Nonlinear optical materials with large and broadband reverse saturable absorption (RSA) and/or two-photon absorption (TPA) are desired for a variety of photonic device applications, such as optical rectification, laser pulse shaping and compression, optical data storage, optical switching, and upconversion lasing.[1−3] A vast amount of organic/organometallic compounds with strong RSA or TPA have been investigated in the past 3 decades, including bis(styryl)benzene derivatives,[4] organic dendrimers,[5,6] metallophthalocyanines,[7] and porphyrins and metalloporphyrins.[8,9]. However, compounds exhibiting broadband RSA or TPA from 400 to 900 nm have been scarce. The limitation lies in the fact that in order to improve the RSA, ground-state absorption in the wavelengths of interest has to be minimized. This can be realized by reducing the π-conjugation in the molecule. However, when the ground-state absorption is too weak or absent, population of the excited states via a one-photon process is correspondingly weak or nonexistent. At the same time, molecules with weak π-conjugation usually have weak two-photon absorption.

Square-planar platinum(II) terdentate or diimine complexes attracted our close attention in recent years as potential broadband nonlinear absorbing materials because of their low ground-state absorption but broad and strong excited-state absorption (ESA) in most of the visible to the near-IR

region.[10−12] The heavy-atom effect of the platinum facilitates the intersystem crossing and gives rise to a high triplet excited state population upon excitation, which enhances the triplet excited-state absorption. These complexes also exhibit excellent thermal and photochemical stability, and it is convenient to conduct structural modifications on these complexes. However, the major limiting factor for utilizing these complexes as broadband nonlinear absorbing materials lies in their very weak ground-state absorption above 550 nm. Recently, our group reported that Pt(II) chloride complexes bearing 4-(9,9-di(2-ethylhexyl)-7-diphenylaminofluoren-2-yl)-2,2′:6′,2″-terpyridine ligand exhibit moderate two-photon absorption in the near-IR region.[13] However, the triplet excited-state absorption from these complexes was too weak to be measured. In further work, however, we synthesized a Pt(II) 2,2′-bipyridine complex bearing 2-(benzothiazol-2′-yl)-9,9-diethyl-7-ethynylfluorene ligands that possesses broadband excited-state absorption in the visible spectral region and large two-photon absorption in the near-IR region.[10] In this complex it is possible to populate the excited state via two-photon absorption in the NIR region. Cooper, Rebane, and Schanze et al. also reported earlier that a

Scheme 1. Synthetic Scheme for Pt(II) Complexes 1 and 2
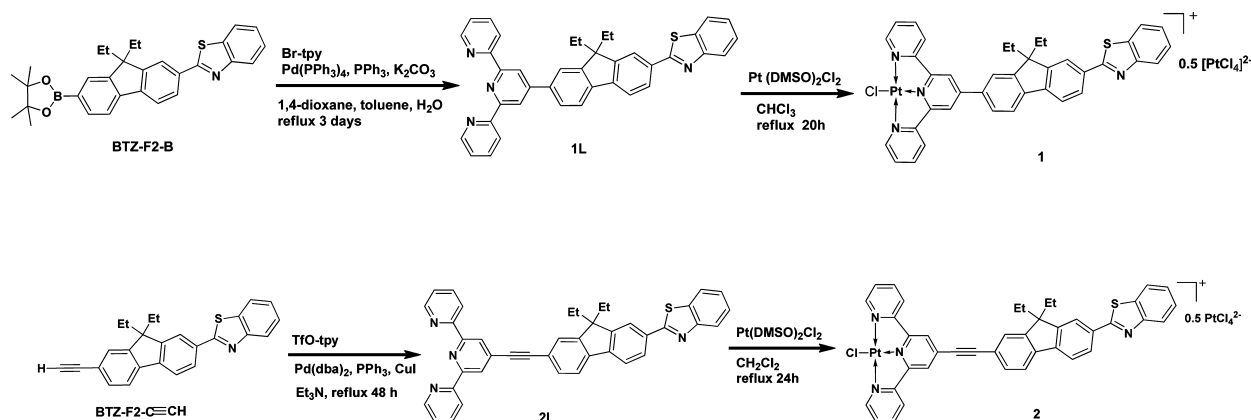
Pt(II) tributylphosphine complex with 2-(benzothiazol-2′-yl)-9,9-diethyl-7-ethynylfluorene ligands exhibited moderately strong two-photon absorption in the NIR region while retaining a broadband excited-state absorption in the visible to the NIR region.[14] To evaluate whether this approach could be applied to platinum terdentate complexes to extend the nonlinear absorption (NLA) spectral range of these complexes as well, in this work we synthesized and studied the nonlinear absorption of two Pt(II) complexes (**1** and **2**) with 4-(7-(benzothiazol-2′-yl)-9,9-diethylfluoren-2-yl)-2,2′:6′,2″-terpyridine ligand (structures shown in Scheme 1). It is well-known that RSA occurs at wavelengths at which the excited-state absorption is stronger than the ground-state absorption, and RSA is enhanced with long excited-state lifetime and high quantum yield of excited state formation. To assess whether complexes **1** and **2** have the potential to be used as RSA materials, photophysical studies including UV−vis absorption, transient absorption, and emission were systematically investigated for these two complexes. It is found that these complexes exhibit strong RSA in the visible spectral region and two-photon-induced excited-state absorption in the near-IR region. Therefore, they are two of the most promising broadband nonlinear absorbing materials reported to date.

2. EXPERIMENTAL SECTION

Synthesis and Characterization. All reagents for synthesis were purchased from Aldrich or Alfa Aesar. Silica gel (200−400 mesh, 60 Å) and alumina gel (activated, neutral, Brockmann I, 150 μm, 58 Å) for column chromatography were from Aldrich. The TLC plates of silica gel (60 Å) and alumina gel (IB-F$_2$) were obtained from Whatman and Baker-Flex Company, respectively. All intermediates were confirmed by ^{1}H NMR spectroscopy, and the ligands **1L**, **2L**, and the Pt(II) complexes **1** and **2** were fully characterized by ^{1}H NMR, high-resolution electrospray ionization mass spectrometry (ESI-MS), and elemental analyses. ^{1}H NMR spectra were measured on a Varian Oxford-400 VNMR spectrometer or a Varian Oxford-500 VNMR spectrometer. ESI-MS analyses were performed on a Bruker BioTOF III mass spectrometer. Elemental analyses were conducted by NuMega Resonance Laboratories, Inc. in San Diego, CA.

The synthetic scheme for complexes **1** and **2** is depicted in Scheme 1. Precursors trifluoromethanesulfonic acid 2,2′;6′,2″-terpyridin-4′-yl ester (TfO-tpy),[15] 2-(9,9-diethyl-7-ethynyl-9H-fluoren-2-yl)-benzothiazole (BTZ-F2-C≡CH),[14] 4′-bromo-2,2′;6′,2″-terpyridine (Br-tpy),[16] and BTZ-F2-B[17] were all prepared following literature procedures. Suzuki coupling reaction of BTZ-F2-B and Br-tpy yielded ligand **1L**. Ligand **2L** was obtained via Sonogashira coupling reaction of BTZ-F2-C≡CH with TfO-tpy. Complexation of **1L** and **2L** with Pt(DMSO)$_2$Cl$_2$ afforded the Pt(II) complexes **1** and **2**.

1L. BTZ-F2-B (0.48 g, 1.0 mmol), Br-tpy (0.32 g, 1.0 mmol), and K$_2$CO$_3$ (5.5 g, 0.04 mol) were dissolved in a degassed mixed solvent of dioxane (40 mL), toluene (40 mL), and water (20 mL). Pd(PPh$_3$)$_4$ (33 mg, 0.03 mmol) and PPh$_3$ (16 mg, 0.06 mmol) were then added. After refluxing for 3 days under argon protection, the aqueous phase was extracted with 50 mL of diethyl ether three times. The organic layers were combined and washed with brine, dried with Na$_2$SO$_4$, and the solvent was removed. The residual solid was purified by chromatography on silica gel. After removal of the byproduct by toluene, the desired product was obtained by elution with dichloromethane or ether. The crude product was recrystallized from dichloromethane and heptane to give 0.37 g of colorless crystal that is suitable for X-ray diffraction analysis (yield, 63%). ^{1}H NMR (400 MHz, CDCl$_3$, δ): 8.79 (s, 2H), 8.73−8.75 (m, 2H), 8.66−8.68 (m, 2H), 8.16 (s, 1H), 8.09 (d, 1H, J = 8.0 Hz), 8.04 (dd, 1H, J = 8.0 and 1.6 Hz), 7.79−7.94 (m, 6H), 7.62−7.68 (m, 1H), 7.42−7.42 (m, 2H), 7.32−7.36 (m, 2H), 2.16−2.26 (m, 4H), 0.37 (t, 6H, J = 7.2 Hz). UV−vis (CH$_2$Cl$_2$): λ$_{max}$ (ε) = 356 (76 390), 372 (sh 56 650). HRMS (ESI, m/z): [M + Na]$^+$ calcd for C$_{39}$H$_{30}$N$_4$SNa, 609.2083; found, 609.2077. Anal. Calcd for C$_{39}$H$_{30}$N$_4$S·CH$_2$Cl$_2$: C, 71.53; H, 4.80; N, 8.34. Found: C, 71.05; H, 5.28; N, 8.36.

2L. BTZ-F2-C≡CH (369 mg, 0.97 mmol) and TfO-tpy (369 mg, 0.97 mmol) were dissolved in degassed triethylamine (50 mL). Pd(dba)$_2$ (15 mg, 0.025 mmol), PPh$_3$ (12 mg, 0.05 mmol), and CuI (5 mg, 0.025 mmol) were then added. After the mixture was refluxed for 2 days under argon, the solvent was removed and the residue was redissolved in CH$_2$Cl$_2$. The CH$_2$Cl$_2$ solution was washed with brine, dried with Na$_2$SO$_4$, and concentrated. The residual solid was purified by chromatography on silica gel. After removal of the byproduct with toluene eluent, the desired product was obtained via CH$_2$Cl$_2$ elution. The crude product was recrystallized from dichloromethane and heptane to give 0.20 g yellow crystal (yield, 33%). ^{1}H NMR (400 MHz, CDCl$_3$, δ): 8.71−8.72 (m, 2H), 8.62 (d, 1H, J = 8.0 Hz), 8.60 (s, 2H), 8.14 (s, 1H), 8.08 (d, 1H, J = 8.0 Hz), 8.04 (dd, 1H, J = 8.0 and 1.6 Hz), 7.90 (d, 1H, J = 8.0 Hz), 7.86 (td, 2H, J = 8.0 and 1.6 Hz), 7.80 (d, 1H, J = 8.0 Hz), 7.76 (d, 1H, J = 8.0 Hz), 7.58 (q, 2H, J = 1.6 Hz), 7.47 (t, 1H, J = 7.2 Hz), 7.38 (t, 1H, J = 8.0 Hz), 7.33−7.35 (m, 2H), 2.10−2.20 (m, 4H), 0.37 (t, 6H, J = 7.2 Hz). UV−vis (CH$_2$Cl$_2$): λ$_{max}$ (ε) = 364 (84 300), 381.5 (68 600). HRMS (ESI, m/z): [M + Na]$^+$ calcd for C$_{41}$H$_{30}$N$_4$SNa, 633.2083; found, 633.2098. Anal. Calcd for C$_{41}$H$_{30}$N$_4$S: C, 80.63; H, 4.95; N, 9.17. Found: C, 80.21; H, 5.30; N, 9.40.

1. Ligand **1L** (510 mg, 0.87 mmol) and Pt(DMSO)$_2$Cl$_2$ (400 mg, 0.96 mmol) were dissolved in CHCl$_3$ (100 mL), and the reaction mixture was refluxed for 24 h under argon. The formed yellow solid was collected by filtration, washed with CH$_2$Cl$_2$ and ether, and dried in vacuum. An amount of 216 mg of orange powder was obtained as the product (yield, 20%). ^{1}H NMR (400 MHz, DMSO, δ): 9.02 (s, 2H), 8.91 (d, 2H, J = 8.0 Hz), 8.87 (br, 2H), 8.53 (t, 2H, J = 7.6 Hz), 8.38 (s, 1H), 8.32 (d, 1H, J = 8.8 Hz), 8.23 (t, 2H, J = 4.0 Hz), 8.18 (t, 1H, J = 8.0 Hz), 8.14 (t, 2H, J = 4.0 Hz), 8.08 (d, 1H, J = 8.0 Hz), 7.91 (t,

2H, J = 6.6 Hz), 7.55 (t, 1H, J = 8.0 Hz), 7.46 (t, 1H, J = 8.0 Hz), 2.29 (m, 4H), 0.31 (t, 6H, J = 7.2 Hz). UV–vis (DMSO): λ_{max} (ε) = 340 (32 550), 378 (20 200), 428 (26 900). HRMS (ESI, m/z): M$^+$ calcd for $C_{39}H_{30}N_4SPtCl$, 817.1528; found, 817.1510. Anal. Calcd for $C_{39}H_{30}ClN_4PtS \cdot 0.5PtCl_4 \cdot 3CH_2Cl_2$: C, 40.66; H, 2.93; N, 4.52. Found: C, 40.70; H, 3.04; N, 4.66.

2. Ligand **2L** (119 mg, 0.20 mmol) and $Pt(DMSO)_2Cl_2$ (93 mg, 0.22 mmol) were dissolved in $CHCl_3$ (50 mL), and the reaction mixture was refluxed for 24 h under argon. The formed orange-red solid was collected by filtration, washed with CH_2Cl_2 and ether, and dried in vacuum. An amount of 32 mg of orange-red powder was obtained as the product (yield, 11%). ^{1}H NMR (400 MHz, DMSO, δ): 8.94 (d, 2H, J = 5.5 Hz), 8.93 (s, 2H), 8.73 (d, 2H, J = 8.0 Hz), 8.56 (dt, 2H, J = 8.0 and 1.5 Hz), 8.26 (s, 1H), 8.19 (d, 1H, J = 8.0 Hz), 8.15 (t, 3H, J = 3.5 Hz), 8.10 (d, 1H, J = 8.0 Hz), 8.00 (t, 2H, J = 8.0 Hz), 7.86 (s, 1H), 7.77 (dd, 1H, J = 8.0 and 1.5 Hz), 7.59 (t, 1H, J = 8.0 Hz), 7.50 (t, 1H, J = 8.0 Hz), 2.15–2.30 (m, 4H), 0.31 (t, 6H, J = 7.0 Hz). UV–vis (DMSO): λ_{max} (ε) = 345 (39 140), 385 (sh 20 140), 433 (27 040). HRMS (ESI, m/z): M$^+$ calcd for $C_{41}H_{30}N_4SPtCl$, 841.1528; found, 841.1575. Anal. Calcd for $C_{41}H_{30}ClN_4PtS \cdot 0.5PtCl_4 \cdot 3.5CH_2Cl_2 \cdot 2DMSO$: C, 39.81; H, 3.38; N, 3.83. Found: C, 39.38; H, 3.29; N, 4.17.

Photophysical Study. The spectroscopic grade solvents used for photophysical experiments were purchased from VWR International and used as is without further purification. The UV–vis absorption spectra in different solvents were measured on an Agilent 8453 spectrophotometer, while the steady-state emission spectra in different solvents were recorded on a SPEX Fluorolog-3 fluorometer/ phosphorometer. The emission quantum yields were determined by the relative actinometry method[18] in degassed solutions, in which a degassed aqueous solution of $[Ru(bpy)_3]Cl_2$ (Φ_{em} = 0.063, λ_{ex} = 436 nm)[19] was used as the reference for complexes **1** and **2** and an aqueous solution of quinine sulfate (Φ_f = 0.60, λ_{ex} = 347.5 nm)[19] was used as the reference for ligands **1L** and **2L**. Time-correlated single photon counting (Edinburgh Instruments OB920 spectrometer) was used to determine emission lifetimes. Samples were excited using a 70 ps laser diode at 375 nm. The emission was detected using a cooled microchannel plate PMT. Data were analyzed using a deconvolution software package provided by Edinburgh Instruments. The time-resolved triplet transient difference absorption spectra and the triplet excited-state quantum yields were measured on an Edinburgh LP920 laser flash photolysis spectrometer in which the third harmonic output (355 nm) of a Nd:YAG laser (Quantel Brilliant, pulsewidth of ~4.1 ns, repetition rate of 1 Hz) was used as the excitation source. Sample solutions were purged with Ar for 30 min prior to each measurement. The triplet excited-state absorption coefficient (ε_T) at the TA band maximum was determined by the singlet depletion method.[20] The triplet quantum yields (Φ_T) were obtained by relative actinometry, in which silicon naphthalocyanine (SiNc) in benzene was used as the reference (ε_{590} = 70 000 M^{-1} cm^{-1}, Φ_T = 0.20).[21] The femtosecond transient difference absorption spectra and the singlet excited-state lifetime were measured using a femtosecond pump–probe UV–vis spectrometer (HELIOS) manufactured by Ultrafast Systems LLC. The sample solution in a 2 mm cuvette was excited at 400 nm using a 150 fs Ti:sapphire laser (Spectra Physics Hurricane, 1 kHz repetition rate, 1 mJ/pulse at 800 nm), and the absorption was probed from 450 to 800 nm with sapphire generated white-light continuum.

Nonlinear Optical Characterization. The nonlinear absorption of complexes **1** and **2** was characterized with an open-aperture Z-scan experiment using a nanosecond laser at 532 nm and a picosecond laser at various wavelengths ranging from 480 to 910 nm and by a nonlinear transmission experiment at 532 nm using a nanosecond laser. For the open-aperture Z-scan measurements, the experimental setup and experimental details were similar to those reported in our previous publications.[10,12,13,22,23] The experimental data were fitted using a five-level model to extract the excited-state absorption cross sections and the two-photon absorption cross sections. The details of the model and fitting procedure were the same as those reported previously.[10,12,13,22,23]

The nonlinear transmission experiment for complexes **1** and **2** was conducted in DMSO in a 2 mm cuvette using 4.1 ns laser pulses at 532 nm. The light source was a Quantel Brilliant nanosecond laser with a repetition rate of 10 Hz. The experimental setup and details are the same as previously described.[11] A 20 cm plano-convex lens was used to focus the beam to the 2 mm thick sample cuvette. The beam waist at the focal plane was 72 μm. The linear transmission of the solution was adjusted to 95% at 532 nm.

3. RESULTS AND DISCUSSION

Electronic Absorption and Emission. Figure 1 shows the UV–vis absorption spectra of **1** and **2** in DMSO solution. The
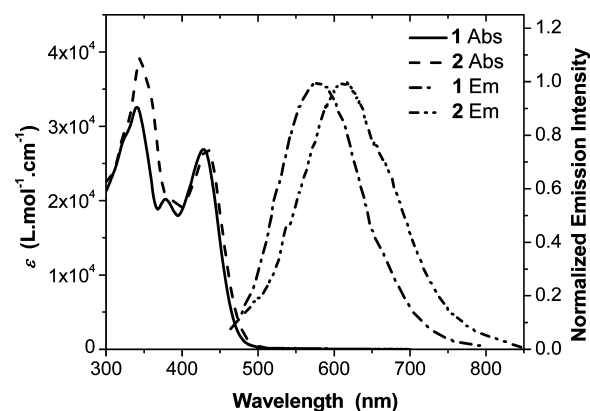

Figure 1. UV–vis absorption and normalized emission spectra of **1** and **2** in DMSO solution. λ_{ex} is 438 nm for **1** and 435 nm for **2**.

absorption of both complexes obeys Beer's law in the concentration range studied (5 × 10^{-6} to 5 × 10^{-4} mol/L). The absorption band maxima and the molar extinction coefficients are listed in Table 1. The band at ~350 nm is assigned to the $^1\pi,\pi^*$ transition of the ligand, which is consistent with the absorption band of the ligands **1L** and **2L** (Supporting Information Figure S1). The absorption band at ~430 nm in **1** and **2** but absent in **1L** and **2L** is attributed to the ^{1}MLCT transition, which exhibits a negative solvatochromic effect as demonstrated in Supporting Information Figure S2 for **1**. Above 500 nm, the linear absorption for both complexes is very weak, which provides a broad optical window for RSA or TPA. The absorption spectrum of **2** is slightly red-shifted compared to that of **1**. This can be explained by the extended π-conjugation in **2**.

Both complexes are weakly emissive at room temperature in solution. Upon excitation at the ^{1}MLCT band, a broad, structureless emission band appears at ~580 nm for **1** and 610 nm for **2** in dilute DMSO solution (Figure 1). The lifetimes were measured via a time correlated single photon counting technique by excitation at 375 nm using a 70 ps diode laser, and the results are listed in Table 1. Considering the remarkable Stokes shift and the negative solvatochromic effect (Figure 2), the emission could be tentatively assigned to a charge-transfer excited state, likely to be the ^{3}MLCT state. However, contribution from the $^3\pi,\pi^*$ state should also be taken into account in view of the unpronounced vibronic structure and the biexponential decay of the emission (Table 1). The longer lifetime could be attributed to the $^3\pi,\pi^*$, while the shorter one could be attributed to the ^{3}MLCT. The probability of the emission emanating from the ^{1}ILCT can be excluded because Zn^{2+}-titration experiment of ligand **1L** shows that the ^{1}ILCT emission appears at 494 nm after ligand complexation with

Table 1. Photophysical Data for 1L, 2L, 1, and 2

	λ_{abs}, nm (ε, L·mol^{-1}·cm^{-1})[a]	λ_{em}, nm (τ_{em}, ps)	Φ_{em}	$\lambda_{S_1-S_n}$, nm (τ_S, ps)	$\lambda_{T_1-T_n}$, nm (ε, L·mol^{-1}·cm^{-1}; τ_T, μs; Φ_T)[d]
1L	359 (70100), 372 (sh 53800)	381, 403 (678), 425 (sh)[b]	0.81[b]	608 (831 ± 78)[b]	570 (76120; 42.6; 0.41)
2L	367 (73900), 385 (61000)	394, 416 (729), 438 (sh)[b]	0.82[b]	644 (655 ± 10)[b]	595 (86030; 48.4; 0.34)
1	340 (32550), 378 (20200), 428 (26900)	581 (50 (39%), 284 (61%))[a]	0.0039[a,c]	542 (49.4 ± 18.3)[a]	530 (48560; 3.37; 0.72)
2	345 (39140), 385 (sh 20140), 433 (27040)	612 (80 (61%), 534 (39%))[a]	0.0068[a,c]	555 (58.7 ± 25.4)[a]	545 (46150; 1.72; 0.58)

[a]In DMSO. [b]In CH$_2$Cl$_2$. [c]Phosphorescence quantum yield. [d]In CH$_3$CN.
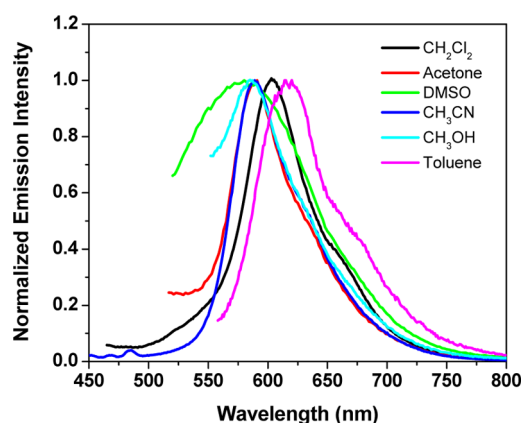

Figure 2. Normalized emission spectra of **1** in different solvents at room temperature. λ_{ex} is 450 nm for CH$_2$Cl$_2$ solution, 424 nm for acetone solution, 438 nm for DMSO solution, 424 nm for CH$_3$CN solution, 422 nm for CH$_3$OH solution, and 467 nm for toluene solution.

Zn^{2+} (Figure 3). Similar to the trend observed for the UV−vis absorption, the emission energy of **2** is lower than that of **1** because of the extended conjugation in the ligand.
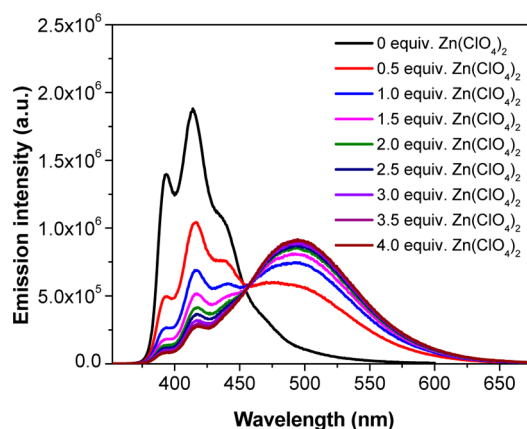

Figure 3. Emission spectra of **1L** in 2.5 × 10^{-5} mol/L DMSO solution at room temperature upon titration with 4.4 × 10^{-2} mol/L Zn(ClO$_4$)$_2$ CH$_3$CN solution. λ_{ex} = 343 nm.

Transient Absorption. To evaluate the feasibility of using **1** and **2** as potential broadband reverse saturable absorbers, the singlet and triplet excited-state absorption characteristics were investigated using femtosecond and nanosecond transient absorption (TA) spectroscopy. For comparison, the femtosecond and nanosecond TAs of **1L** and **2L** were also studied. Figure 4a presents the nanosecond TA spectra for **1L**, **2L**, **1**, and **2** in CH$_3$CN solution at zero delay after excitation at 355 nm, and the time-resolved nanosecond TA spectra of **1** are
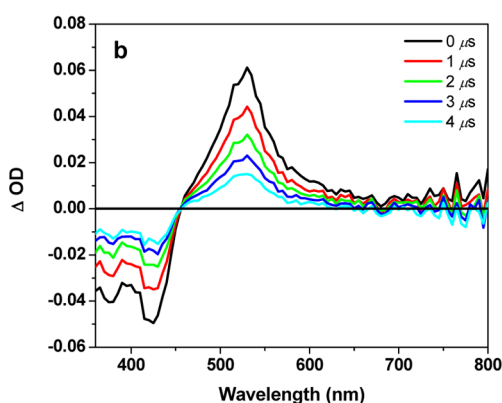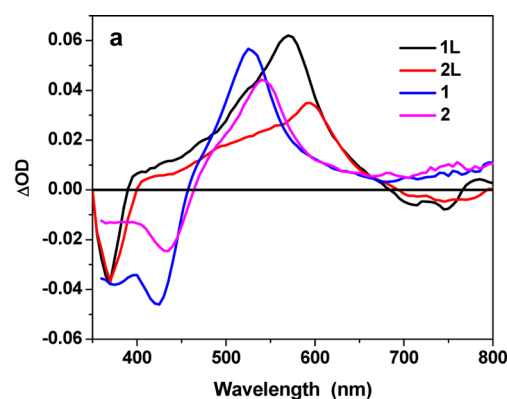

Figure 4. (a) Nanosecond transient difference absorption spectra of **1L**, **2L**, **1**, and **2** in CH$_3$CN solution immediately after 355 nm laser excitation. A_{355} = 0.4 in a 1 cm cuvette. (b) Time-resolved nanosecond transient difference absorption spectra of **1** in CH$_3$CN solution. λ_{ex} = 355 nm. A_{355} = 0.4 in a 1 cm cuvette.

shown in Figure 4b. The time-resolved nanosecond TA spectra of **1L**, **2L**, and **2** are given in Supporting Information Figure S3. It is obvious that the TA spectral features of the platinum complexes are quite similar to those of their ligands, with a negative absorption band appearing below 400 nm and a relatively broad positive band above 500 nm. The position of the negative band is consistent with the UV−vis absorption band maximum, indicating a bleaching of the ground-state absorption in this region. In view of the long lifetimes deduced from the decay of the TA, the excited state that gives rise to the nanosecond TA is attributed to the $^3\pi,\pi^*$ state. Consistent with the trend observed from the UV−vis absorption and emission studies, the absorption band maxima of **2L** and **2** are all red-shifted compared to those of **1L** and **1**, and the $\varepsilon_{T_1-T_n}$ values are significantly enhanced for **2L** and **2**. Again, this is attributed to the extended conjugation by insertion of the triple bond in **2L** and **2**. The shorter lifetimes of **1** and **2** compared to their respective ligand should be ascribed to the rapid decay from T$_1$ to S$_0$ due to heavy atom induced intersystem crossing.

The femtosecond TA spectra of **1** and **2** (Supporting Information Figure S4) resemble their respective nanosecond TA spectra, indicating a rapid intersystem crossing from the singlet excited state to the triplet excited state, which is typical for Pt complexes because of the heavy-atom enhanced spin−orbit coupling. In contrast, the transition from the singlet to triplet excited state is clearly evident in the time-resolved femtosecond TA spectra of **1L** and **2L**. As exemplified in Figure 5 for **1L**, a strong absorption band appears at 608 nm
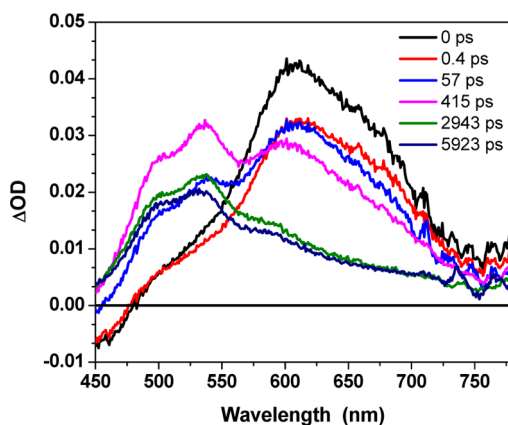

Figure 5. Time-resolved femtosecond transient difference absorption spectra of **1L** in CH$_2$Cl$_2$ solution. λ_{ex} = 400 nm.

immediately after the laser excitation. This band decays rapidly with a new band occurring at ~536 nm after 57 ps of excitation, which is the similar position as the nanosecond TA band maximum. Approximately 2.9 ns after excitation, the original 608 nm band almost completely disappears, and the new band at 536 nm reaches the maximum intensity, which then decays slowly. **2L** exhibits the similar transition from the singlet excited state to the triplet excited state after ~74 ps of excitation.

Reverse Saturable Absorption. Because complexes **1** and **2** exhibit relatively broad and strong excited-state absorption in the visible spectral region upon both nanosecond and femtosecond laser excitation, reverse saturable absorption (RSA) from **1** and **2** is expected to be observed in the visible spectral region. To demonstrate this, nonlinear transmission measurements of **1** and **2** in DMSO solution in a 2 mm cuvette were performed using 532 nm, 4.1 ns laser pulses, and the results are presented in Figure 6. The linear transmission of the solution was adjusted to 95% in the 2 mm cuvette. Drastic transmission decrease was observed for both **1** and **2** when the incident energy increased, which is a clear indication of strong RSA. The RSA of **1** is slightly stronger than that of **2**.

Z-Scan and Two-Photon Absorption. To rationalize the observed RSA of **1** and **2** at 532 nm, obtain numerical values for their respective singlet and triplet excited-state absorption cross sections, and quantify the strength of the two-photon absorption in the near-IR, Z-scan experiments[24] were carried out at 532 nm using both nanosecond and picosecond laser pulses and at a variety of other wavelengths between 430 and 910 nm using picosecond laser pulses. The experimental data were fitted by a five-level model[22,23] that tracks the relative population of the ground state (S$_0$), the first and second singlet excited states (S$_1$ and S$_2$), and the first and higher triplet excited states (T$_1$ and T$_n$). The ground-state absorption cross sections as a function of wavelength obtained from the UV−vis spectra of the two complexes, the singlet and triplet excited-
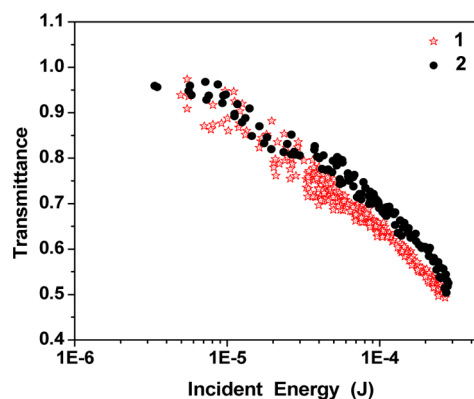

Figure 6. Nonlinear transmission curves of **1** and **2** in DMSO solution for 4.1 ns laser pulses at 532 nm. The linear transmission of the solution was adjusted to 95% in a 2 mm cuvette. The beam waist at the focal plane was 72 μm.

lifetimes obtained from the decay of the femtosecond and nanosecond TA, and the triplet quantum yields obtained from the actinometry method were used as input parameters for the fittings. The singlet and triplet excited-state absorption cross sections at 532 nm were obtained by fitting the nanosecond and picosecond Z-scan data simultaneously. The effective triplet excited-state absorption cross sections $\sigma_T(\lambda)$ at the other wavelengths were deduced from the femtosecond TA curve at 5.9 ns time delay in combination with the value of σ_T at 532 nm. Detailed descriptions of the model and the fitting process were reported by our group previously.[10,12,13,22,23]

Figure 7a shows the picosecond Z-scan experimental data and fitting curves for **2** at 500 nm. A drastic transmission decrease is observed when the sample is moved toward the linear focal plane, which is a clear indication of RSA. The ground-state absorption cross sections and the singlet and triplet excited-state absorption cross sections in the visible spectral region for **1** and **2** are provided in Table 2. At wavelengths longer than 600 nm for **1** and 630 nm for **2**, these two complexes exhibit very weak or nonmeasurable ground-state absorption, and population of the excited states via one-photon absorption becomes very weak or impossible. However, significant transmission reduction was still clearly evident at these wavelengths. This indicates that both **1** and **2** exhibit two-photon absorption in the near-IR region, which serves to populate the excited states and open the possibility of subsequent excited-state absorption. Two-photon absorption cross sections deduced from the fitting of the Z-scan data are also provided in Table 2. The ratios of the excited-state to ground-state absorption cross sections at different visible wavelengths for **1** and **2** are given in Table 2 and plotted in Figure 7b. It is quite obvious that both the σ_s/σ_0 and σ_T/σ_0 values are much higher for **1** than **2** because of the reduced ground-state absorption of **1**. However, unlike the trend of σ_{ex}/σ_0, the two-photon absorption cross sections (σ_2) for **2** are much larger than those of **1**. The enhanced two-photon absorption in **2** can be attributed to the increased conjugation by the triple bond connection, which not only increases the conjugation length but also makes the benzothiazolylfluorenyl component more coplanar with the terpyridine ligand. The latter would significantly enhance the π-electron interaction and delocalization between the benzothiazolylfluorenyl component and the terpyridine component. Both of these factors, especially the latter one, contribute to the dramatically enhanced σ_2 in **2**.
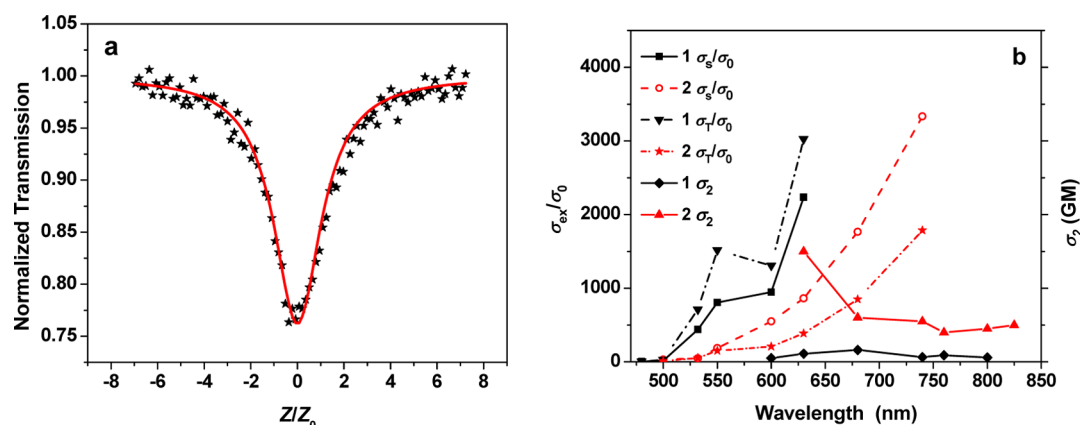
Figure 7. (a) Picosecond Z-scan experimental data (symbol) and theoretical fitting curve (solid line) for **2** at 500 nm in DMSO solution. The concentration used for the measurement was 4.2×10^{-4} mol/L, and the path length of the cuvette was 2 mm. The laser energy was 4.5 μJ, and the radius of the beam waist at the focal plane was 33 μm. (b) Wavelength dispersion of the ratios of excited-state absorption cross section to that of the ground-state absorption (σ_{ex}/σ_0) and two-photon absorption cross section (σ_2) for **1** and **2** in DMSO solution.

Table 2. Absorption Cross Sections of 1 and 2 at Selected Wavelengths Determined by Fitting of Z-Scan Data Except Where Indicated

	$\sigma_0(\lambda)^a/10^{-18}$ cm²		$\sigma_S(\lambda)/10^{-18}$ cm²		$\sigma_T(\lambda)^c/10^{-18}$ cm²		σ_S/σ_0		σ_T/σ_0		$\sigma_2(\lambda)$/GM	
λ/nm	1	2	1	2	1	2	1	2	1	2	1	2
480	5.23		28		28		5.35		5.35			
500	1.41	1.32	22	42	40	14	15.6	31.8	28.4	10.6		
532	0.0955	0.390	42	19	68	21	440	48.7	712	53.8		
550	0.0435	0.187	35	35	66	28	805	187	1517	150		
600	0.0222	0.0726	21^b	40	29	15	946	551	1306	207	50	
630	0.0076	0.0336	17^b	29^b	23	13	2237	863	3026	387	110	1500
680	~0	0.0153	19^b	27^b	23	13		1765		850	160	600
740	~0	0.0084	22^b	28^b	31	15		3333		1786	65	550
760	~0	~0	22^b	29^b	36	16					90	400
800	~0	~0	22^b	23^b	53	20					60	450
825	~0	~0		43^b		21					200^d	500
850	~0	~0									280^d	3700^e
875	~0	~0									180^d	3000^e
900	~0										200^d	
910	~0	~0										1700^e

^{a}From UV−vis absorption spectrum. ^{b}Estimated from $\sigma_S(532$ nm) and the femtosecond transient difference absorption spectrum at zero time delay. Because the femtosecond TA will include contributions from both S$_1$ and S$_2$, these values should be considered *effective* cross sections for the singlet excited states. $^c\sigma_T(532$ nm) was determined from combined fitting of nanosecond and picosecond Z-scan data. For other wavelengths, $\sigma_T(\lambda)$ was estimated from $\sigma_T(532$ nm) and the femtosecond transient difference absorption spectrum at 5.9 ns time delay. ^{d}Effective two-photon absorption cross section for excited-state-assisted two-photon absorption. ^{e}Effective two-photon absorption cross section for the Z scan of lowest energy (11.5 μJ at 825 nm, 7.9 μJ at 850 nm, 8.3 μJ at 875 nm, and 10.0 μJ at 900 nm). At each wavelength, Z scans at a progression of higher energies yield higher effective σ_2 values, clear evidence for two-photon-initiated excited-state absorption.

The enhancement of TPA cross section with increased π-conjugation length or coplanarity has been well studied in squaraine dyes,[25,26] metalloporphyrins,[27] and other organic compounds.[28] This enhancement has also been reported by our group for Pt(II) terpyridine complexes bearing a diphenylaminofluorenyl substituent.[13] However, the triple bond linkage only gives less than 2 times enhancement of the σ_2 values than the one lacking of triple bond linkage for the complexes containing a diphenylaminofluorenyl substituent. The dramatic enhancement of the σ_2 values in **2** than in **1** could possibly be attributed to the following three factors: First, it is well-known that the σ_2 values obtained by Z scan method could be overestimated compared to those obtained by the two-photon excited fluorescence method; however, because of the lack of a femtosecond laser source, we are unable to verify this at this time. However, the overestimation by Z-scan method is a

systematic error and it applies to the σ_2 values of both **1** and **2**. We think that even if the overestimation by Z-scan method exists, it should not be the dominant contributor to the much larger σ_2 values in **2** than in **1**. Second, the solubility of **2** is lower than **1** in organic solvents including DMSO. Although we took a great care to get the most accurate ground-state absorption cross sections at longer wavelengths (>630 nm) using a saturated DMSO solution of **2** in a 1 cm cuvette, the uncertainty at longer wavelengths for **2** could still possibly be larger than that for **1**. Therefore, the much larger σ_2 values in **2** could possibly be inflated somewhat by the underestimated contribution from the unmeasurably small inaccuracy in single-photon ground-state absorption. Third, the nature of the lowest excited state of **1** and **2**, which is dominated by MLCT character, is quite different from the intramolecular charge transfer (ILCT) dominated lowest excited state in complexes

Table 3. Comparison of the Two-Photon Absorption Cross Sections of 1 and 2 to Selected Pt(II) Complexes

	σ_2/GM						
λ/nm	1 in this work (21 ps, Z scan)	2 in this work (21 ps, Z scan)	1 in ref 17 (21 ps, Z scan)	1 in ref 10 (21 ps, Z scan)	2 in ref 13 (21 ps, Z scan)	1 in ref 14 (100 fs, fluo)	PE2
595	50 (at 600 nm)					210	235 (27 ps, Z scan)[35]
630	110	1500		1000			
680	160	600		400			
720						370	7 (180 fs, Z scan)[36]
740	65	550	600	600	1200		
760	90	400		1000	1000		
800	60	450	650	300	2000		
825	200[a]	500		80	600		
850	280[a]	3700[d]	1200[b]	600[a]			
875	180[a]	3000[d]	220[c]	300[a]			
910	200[a] (at 900 nm)	1700[d]	200[c]	300[a]			

[a]Effective cross-section for excited-state-assisted two-photon absorption. [b]Effective two-photon absorption cross section for the Z scan of lowest energy (0.5 J/cm^2). Z scans at a progression of higher energies (0.7 and 1.1 J/cm^2) yield effective σ_2 values of 1900 and 2000 GM, respectively, clear evidence for two-photon-initiated excited-state absorption. [c]Effective two-photon absorption cross section for the Z scan of 0.3 J/cm^2 fluence on axis. [d]Effective two-photon absorption cross section for the Z scan of lowest energy (11.5 μJ at 825 nm, 7.9 μJ at 850 nm, 8.3 μJ at 875 nm, and 10.0 μJ at 900 nm). At each wavelength, Z scans at a progression of higher energies yield higher effective σ_2 values, clear evidence for two-photon-initiated excited-state absorption.

bearing diphenylaminofluorenyl substituent.[13] We speculate this could be the major reason that causes the different degree of enhancement in 2 by the triple bond linkage compared to the complex with diphenylaminofluorenyl substituent. Above 825 nm, the TA could not be measured because of the detection limit of our spectrometer. Thus, we are unable to estimate the singlet and triplet excited-state absorption cross sections at the wavelengths of 825–910 nm, and the two-photon absorption cross sections reported in Table 2 for these wavelengths are effective cross sections for excited-state-assisted two-photon absorption.

It is noted that two-photon initiated excited-state absorption has been reported for fluorene-based organic molecules[29,30] and stilbene derivatives,[31] and some of them show strong apparent nonlinear transmission in the near-IR region. However, the reported nonlinear transmission curves were conducted at different wavelengths than 532 nm (the wavelength we used to demonstrate nonlinear transmission of our complexes), it is not reasonable to compare the nonlinear transmission of nonlinear absorbing materials at different measurement conditions. Rather than that, the intrinsic molecular parameters, such as the ratios of the excited-state absorption cross section relative to that of the ground state for reverse saturable absorbers and σ_2 for two-photon absorbers, should be compared. Both the σ_S/σ_0 and σ_T/σ_0 values for 1 and 2 (Table 2) are among the largest values reported to date for reverse saturable absorbers at each of the corresponding wavelength in the visible to the near-IR region (see Supporting Information Tables S1 and S2 for comparison).[10,11,13,17,23,32–34] In addition, the σ_2 values for 1 and 2 are comparable or better than the values reported in the literature for fluorene-based organic molecules[22,23] (note that the σ_2 values reported in the literature are effective TPA cross sections, which include contributions from both TPA and ESA and thus are larger than the true σ_2 as we deduced for 1 and 2 in this paper). Nonetheless, the σ_2 values for 1 and 2 are among the largest values for Pt(II) complexes reported to date (see Table 3 for comparison)[10,13,14,17,35–41] and the nonlinear absorption spectral region (480–910 nm considering both RSA and TPA region) is greatly expanded compared to the fluorene-based organic molecules and stilbene derivatives.[29–31]

It is also worth mentioning that (polypyridyl)metal-(porphinato)zinc(II) compounds exhibit broad ESA.[42,43] However, the ESA is primarily in the near-IR region, which is different from the ESA region for 1 and 2 that covers most of the visible spectral region. Therefore, it is not appropriate to compare the ESA of 1 and 2 with (polypyridyl)metal-(porphinato)zinc(II) compounds either.

4. CONCLUSION

Two Pt(II) complexes bearing a 7-(benzothiazol-2′-yl)-9,9-diethylfluoren-2-yl substituent on the 4-position of terpyridine ligand via single or triple bond connection were synthesized, and their photophysical properties and nonlinear absorption were systematically investigated. Both complexes exhibit strong ^{1}MLCT transition at ~430 nm and weak ^{3}MLCT/$^3\pi,\pi^*$ emission at ~600 nm. The excited-state absorption of both complexes is quite strong and relatively broad in the visible spectral region. Therefore, both complexes show strong RSA in the visible region, with very large ratios of σ_{ex}/σ_0 values. Z-Scan experiments reveal that these complexes exhibit two-photon initiated excited-state absorption in the near-IR region. The TPA cross sections for 2 are among the largest values reported for Pt(II) complexes. Thus, both of them are promising broadband nonlinear absorbing materials. It is also found that complex 2 with the triple bond connection between the fluorenyl component and the terpyridine ring has a red-shifted UV–vis absorption, emission, and transient absorption, as well as significantly larger TPA compared to those of 1, due to the extended conjugation by the triple bond.

■ ASSOCIATED CONTENT

Ⓢ Supporting Information

UV–vis absorption spectra of 1L and 2L in DMSO solution, normalized UV–vis absorption spectra of 1 in different solvents, time-resolved nanosecond transient difference absorption spectra of 1L, 2L, and 2 in CH$_3$CN solution, and time-resolved femtosecond transient difference absorption spectra of 2L in CH$_2$Cl$_2$ and 1 and 2 in DMSO solution. This material is available free of charge via the Internet at http://pubs.acs.org.

■ AUTHOR INFORMATION

Corresponding Author
*E-mail: Wenfang.Sun@ndsu.edu. Phone: 701-231-6254.

Notes
The authors declare no competing financial interest.

■ REFERENCES

(1) Sutherland, R. L. In *Handbook of Nonlinear Optics*; Marcel Dekker, Inc.: New York, NY, U.S., 1996; Chapters 9 and 11.

(2) Pawlicki, M.; Collins, H. A.; Denning, R. G.; Anderson, H. L. *Angew. Chem., Int. Ed.* **2009**, *48*, 3244.

(3) He, G. S.; Tan, L.-S.; Zheng, Q.; Prasad, P. N. *Chem. Rev.* **2008**, *108*, 1245.

(4) Albota, M.; Beljonne, D.; Brédas, J.-L.; Ehrlich, J. E.; Fu, J.-Y.; Heikal, A. A.; Hess, S. E.; Kogej, T.; Levin, M. D.; Marder, S. R.; McCord-Maughon, D.; Perry, J. W.; Rockel, H.; Rumi, M.; Subramaniam, G.; Webb, W. W.; Wu, X.-L.; Xu, C. *Science* **1998**, *281*, 1653.

(5) McDonagh, A. M.; Humphrey, M. G.; Samoc, M.; Luther-Davies, B. *Organometallics* **1999**, *18*, 5195.

(6) Drobizhev, M.; Karotki, A.; Rebane, A.; Spangler, C. W. *Opt. Lett.* **2001**, *26*, 1081.

(7) Perry, J. W.; Mansour, K.; Marder, S. R.; Perry, K. J.; Alvarez, D., Jr.; Choong, I. *Opt. Lett.* **1994**, *19*, 625.

(8) Perry, J. W. In *Nonlinear Optics of Organic Molecules and Polymers*; Nalwa, H. S., Miyata, S., Eds.; CRC: Baca Raton, FL, U.S., 1997; Chapter 13.

(9) Frampton, M. J.; Akdas, H.; Cowley, A. R.; Rogers, J. E.; Slagle, J. E.; Fleitz, P. A.; Drobizhev, M.; Rebane, A.; Anderson, H. L. *Org. Lett.* **2005**, *7*, 5365.

(10) Sun, W.; Zhang, B.; Li, Y.; Pritchett, T. M.; Li, Z.; Haley, J. E. *Chem. Mater.* **2010**, *22*, 6384.

(11) Guo, F.; Sun, W.; Liu, Y.; Schanze, K. *Inorg. Chem.* **2005**, *44*, 4055.

(12) Shao, P.; Li, Y.; Yi, J.; Pritchett, T. M.; Sun, W. *Inorg. Chem.* **2010**, *49*, 4507.

(13) Ji, Z.; Li, Y.; Pritchett, T. M.; Makarov, N. S.; Haley, J. E.; Li, Z.; Drobizhev, M.; Rebane, A.; Sun, W. *Chem.—Eur. J.* **2011**, *17*, 2479.

(14) Rogers, J. E.; Slagle, J. E.; Krein, D. M.; Burke, A. R.; Hall, B. C.; Fratini, A.; McLean, D. G.; Fleitz, P. A.; Cooper, T. M.; Drobizhev, M.; Makarov, N. S.; Rebane, A.; Kim, K.-Y.; Farley, R.; Schanze, K. S. *Inorg. Chem.* **2007**, *46*, 6483.

(15) Potts, K. T.; Konwar, D. *J. Org. Chem.* **1991**, *56*, 4815.

(16) Leslie, W.; Batsanov, A. S.; Howard, J. A. K.; Gareth Williams, J. A. *Dalton Trans.* **2004**, 623.

(17) Zhang, B.; Li, Y.; Liu, R.; Pritchett, T. M.; Azenkeng, A.; Haley, J. E.; Ugrinov, A.; Li, Z.; Hoffmann, M. R.; Sun, W. *Chem.—Eur. J.* **2012**, *18*, 4593.

(18) Demas, J. N.; Crosby, G. A. *J. Phys. Chem.* **1971**, *75*, 991.

(19) Suzuki, K.; Kobayashi, A.; Kaneko, S.; Takehira, K.; Yoshihara, T.; Ishida, H.; Shiina, Y.; Oishi, S.; Tobita, S. *Phys. Chem. Chem. Phys.* **2009**, *11*, 9850.

(20) Carmichael, I.; Hug, G. L. *J. Phys. Chem. Ref. Data* **1986**, *15*, 1.

(21) Firey, P. A.; Ford, W. E.; Sounik, J. R.; Kenney, M. E.; Rodgers, M. A. J. *J. Am. Chem. Soc.* **1988**, *110*, 7626.

(22) Li, Y.; Pritchett, T. M.; Huang, J.; Ke, M.; Shao, P.; Sun, W. *J. Phys. Chem. A* **2008**, *112*, 7200.

(23) Pritchett, T. M.; Sun, W.; Guo, F.; Zhang, B.; Ferry, M. J.; Rogers-Haley, J. E.; Shensky, W., III; Mott, A. G. *Opt. Lett.* **2008**, *33*, 1053.

(24) Sheik-Bahae, M.; Said, A. A.; Wei, T.-H.; Hagen, D. J.; Van Stryland, E. W. *IEEE J. Quantum Electron.* **1990**, *26*, 760.

(25) Chung, S.-J.; Zheng, S.; Odani, T.; Beverina, L.; Fu, J.; Padilha, L. A.; Biesso, A.; Hales, J. M.; Zhan, X.; Schmidt, K.; Ye, A.; Zojer, E.; Barlow, S.; Hagan, D. J.; Van Stryland, E. W.; Yi, Y.; Shuai, Z.; Pagani, G. A.; Brédas, J.-L.; Perry, J. W.; Marder, S. R. *J. Am. Chem. Soc.* **2006**, *128*, 14444.

(26) Beverina, L.; Crippa, M.; Salice, P.; Ruffo, R.; Ferrante, C.; Fortunati, I.; Signorini, R.; Mari, C. M.; Bozio, R.; Facchetti, A.; Pagani, G. A. *Chem. Mater.* **2008**, *20*, 3242.

(27) Drobizhev, M.; Stepanenko, Y.; Dzenis, Y.; Karotki, A.; Rebane, A.; Taylor, P. N.; Anderson, H. L. *J. Phys. Chem. B* **2005**, *109*, 7223.

(28) Ventelon, L.; Charier, S.; Moreaux, L.; Mertz, J.; Blanchard-Desce, M. *Angew. Chem., Int. Ed.* **2001**, *40*, 2098.

(29) Sutherland, R. L.; Brant, M. C.; Heinrichs, J.; Rogers, J. E.; Slagle, J. E.; McLean, D. G.; Fleitz, P. A. *J. Opt. Soc. Am. B* **2005**, *22*, 1939.

(30) Belfield, K. D.; Bondar, M. V.; Hernandez, F. E.; Przhonska, O. V.; Yao, S. *J. Phys. Chem. B* **2007**, *111*, 12723.

(31) Ehrlich, J. E.; Wu, X. L.; Lee, I.-Y. S.; Hu, Z.-Y.; Rockel, H.; Marder, S. R.; Perry, J. W. *Opt. Lett.* **1997**, *22*, 1843.

(32) Sun, W.; Li, Y.; Pritchett, T. M.; Ji, Z.; Haley, J. E. *Nonlinear Opt., Quantum Opt.* **2010**, *40*, 163.

(33) Song, Y.; Fang, G.; Wang, Y.; Liu, S.; Li, C.; Song, L.; Zhu, Y.; Hu, Q. *Appl. Phys. Lett.* **1999**, *74*, 332.

(34) Si, J.; Yang, M.; Wang, Y.; Zhang, L.; Li, C.; Wang, D.; Dong, S.; Sun, W. *Appl. Phys. Lett.* **1994**, *64*, 3083.

(35) Staromlynska, J.; McKay, T. J.; Bolger, J. A.; Davy, J. R. *J. Opt. Soc. Am. B* **1998**, *15*, 1731.

(36) Vestberg, R.; Westlund, R.; Eriksson, A.; Lopes, C.; Carlsson, M.; Eliasson, B.; Glimsdal, E.; Lindgren, M.; Malmstrom, E. *Macromolecules* **2006**, *39*, 2238.

(37) Kim, K.-Y.; Shelton, A. H.; Drobizhev, M.; Makarov, N.; Rebane, A.; Schanze, K. S. *J. Phys. Chem. A* **2010**, *114*, 7003.

(38) Chan, C. K. M.; Tao, C.-H.; Tam, H.-L.; Zhu, N.; Yam, V. W.-W.; Cheah, K.-W. *Inorg. Chem.* **2009**, *48*, 2855.

(39) McKay, T. J.; Staromlynska, J.; Wilson, P.; Davy, J. *J. Appl. Phys.* **1999**, *85*, 1337.

(40) Glimsdal, E.; Carlsson, M.; Eliasson, B.; Minaev, B.; Lindgren, M. *J. Phys. Chem. A* **2007**, *111*, 244.

(41) Westlund, R.; Glimsdal, E.; Lindgren, M.; Vestberg, R.; Hawker, C.; Lopes, C.; Malmström, E. *J. Mater. Chem.* **2008**, *18*, 166.

(42) Duncan, T. V.; Rubtsov, I. V.; Uyeda, H. T.; Therien, M. J. *J. Am. Chem. Soc.* **2004**, *126*, 9474.

(43) Duncan, T. V.; Ishizuka, T.; Therien, M. J. *J. Am. Chem. Soc.* **2007**, *129*, 9691.